RSC Advances

ROYAL SOCIETY OF CHEMISTRY

www.rsc.org/advances

Flexible Hard Nanocomposite Coatings

J.Musil

Department of Physics and NTIS – European Centre of Excellence, University of West Bohemia
Univerzitni 8, CZ-30614 Plzen, Czech Republic
phone: +420 37763 2200, fax: +420 37763 2202
e-mail: musil@kfy.zcu.cz

Abstract

The article reports on flexible hard nanocomposite coatings prepared by magnetron sputtering. It is shown that the flexible hard nanocomposite coatings (i) represent a new class of coatings which are simultaneously hard, tough and resistant to cracking, (ii) exhibit high values of the hardness H and the effective Young's modulus E^* ratio $H/E^* \geq 0.1$, the elastic recovery $W_e \geq 60\%$, compressive macrostress $\sigma < 0$ and dense, voids-free microstructure, and (iii) are formed in the zone T of the Thornton's Structural Zone Model (SZM); here $E^* = E/(1 - \nu^2)$, E is the Young's modulus and ν is the Poisson's ratio. The magnetron sputtering, which is a very powerful process used in the preparation of nanocomposite coatings, is described in detail. The basic principles of the formation of flexible hard coatings are also described in detail. It is shown that key parameters which decide on the formation of these coatings are (1) the energy $\varepsilon_p = \varepsilon_{ca} + \varepsilon_{bi}$ delivered to the growing coating by condensing atoms (ε_{ca}) and bombarding ions (ε_{bi}) (the non-equilibrium heating), (2) the substrate heating controlled by the substrate temperature T_s (the equilibrium heating) and (3) the melting temperature T_m of the coating material. The flexible hard coatings represent a huge application potential. Four examples of flexible coatings are given: (1) flexible protective coatings, (2) flexible functional coatings, (3) flexible over-layer preventing cracking of brittle coating and (4) flexible multilayer coating. Also, the principle of a low-temperature sputtering of flexible nanocomposite coatings is described in detail. At the end, trends of next development of the nanocomposite coatings with unique properties are given.

Keywords: Hard nanocomposite coatings, Microstructure, Macrostress, Mechanical properties, Energy, Flexibility, Resistance to cracking, Magnetron sputtering

Content

1. Introduction

Hard nanocomposite coatings represent a new generation of coatings [1-44 and references therein]. Typical example of the hard nanocomposite coatings is the two-phase nc-TiN/a-Si_3N_4 composite. Main advantage of the

hard nanocomposite coatings is an enhanced hardness H. Therefore, at first, main attention was devoted to the explanation of the origin of enhanced hardness H of the nanocomposite coating and to the achievement of its as high possible hardness H. The nanocomposite coatings with hardness H > 40 GPa are called the superhard nanocomposite coatings. At present, there are two big groups of two-phase nanocomposite coatings with enhanced hardness H: (1) hard phase/hard phase nanocomposites and (2) hard phase/soft phase nanocomposites [10,41,42]. Here it is necessary to underline that (i) both groups of the nanocomposite coatings can exhibit the enhanced hardness H and (ii) the second group, i.e. the hard phase/soft phase nanocomposites, can exhibit also further unique physical and functional properties.

Very important is also thermal stability and oxidation resistance of the nanocomposite coatings at high temperatures T above 1000 °C. Recently, two kinds of X-ray amorphous hard coatings– (1) the nc-TMN/a-Si_3N_4 composite coatings with high (> 20 at.%) Si content and (2) the Si-B-C-N coatings with covalent bonds – thermally stable and oxidation resistant up to ~ 1500 and ~1700°C, respectively, – were successfully developed [34]. Besides, it was understood that the enhanced hardness H is not a single important property of the hard nanocomposite coatings. For many applications the toughness of the hard coating is more important than its extremely high hardness H considerably exceeding 40 GPa. Therefore, at present, a great attention is concentrated on the development of the flexible coatings which are simultaneously hard, tough and resistant to cracking in bending [41,44-52]. These coatings represent a huge potential for many new advanced applications, for instance, in the flexible electronics, the flat panel displays, the micro-electro-mechanical systems (MEMS), the formation of functional coatings on flexible substrates such polymer foils, thin sheet glass, textile etc.

The development of flexible nanocomposite coatings is a subject of this article. It reports on a new class of advanced flexible hard coatings with enhanced resistance to cracking prepared by reactive magnetron sputtering. This article shows (i) the correlations between the coating microstructure, mechanical properties of coatings (the hardness H, the effective Young's modulus E^*, the elastic recovery W_e and macrostress σ and the energy ε delivered to the growing coating, (ii) the conditions under which the flexible hard nanocomposite coatings can be formed, (iii) how cracking of brittle coatings can be prevented, (iv) four examples of flexible hard coatings and (v) the principle of low-temperature sputtering of flexible coatings; here the effective Young's modulus $E^* = E/(1 - \nu^2)$, E is the Young's modulus and ν is the Poisson's ratio. At the end, the trends of next development are outlined.

2. Magnetron sputtering of nanocomposite coatings

The magnetron sputtering is a very efficient tool for the formation of nanocomposite coatings [53-80]. Today, this method is well mastered and the sputtering of coatings can be realized in direct current (DC), radio frequency (RF), and DC or AC pulse mode of sputtering process; here the AC pulse is the pulse composed of negative half-sinusoids. The DC sputtering is used for the deposition of metallic and electrically conductive coatings. The RF and pulsed sputtering is suitable particularly for sputtering of electrically insulating coatings. The sputtering of coatings can be realized in pure argon or in a mixture of argon and reactive gas (RG). In the first case the coatings containing elements of sputter target can be formed. The sputtering of coatings in a mixture of argon and reactive gas is called *reactive magnetron sputtering*.

The reactive magnetron sputtering is very important process because it forms coatings containing not only elements of sputtered target but also elements of reactive gas. This way the compound coatings such as nitrides, oxides, carbides, borides, chlorides, etc., and their combinations can be formed. However, the reactive magnetron sputtering can exhibit two undesirable effects: (1) the hysteresis effect and (2) arcing on the surface of sputtered target. The both effects occur in consequence of a poisoning of the sputtered target and need to be eliminated to form defects free coatings in a reproducible way. The hysteresis effect can be eliminated in the case when the pumping speed for the reactive gas S_{RG} is greater than a critical pumping speed of the pumping system of deposition device [55]. The arcing on the sputtered target occurs when electrically insulating coatings are sputtered in consequence of charging of insulating layers formed on its uneroded areas. There are two ways allowing eliminate the arcing: (1) to use magnetrons with full target erosion (not perfectly mastered yet) or (2) to remove the accumulated charge from insulated layers on uneroded areas [56, 80]. Very efficient tool removing accumulated charge from the sputtered target is pulsed sputtering with a positive voltage on the target during pulsed off time. Typical example of such pulsed sputtering system is the dual magnetron operating in bipolar mode [63,77,80]. The principle of the dc pulse dual magnetron sputtering is displayed in Fig.1. The voltage polarity of magnetron cathodes periodically changes from negative to positive. When the cathode voltage U_d is negative the target material is sputtered. On the contrary, when U_d is positive the charge accumulated at the surface of insulating layer formed on the uneroded areas of target is discharged as a result of the electron bombardment. Here, it is also worthwhile to note that a distribution of the discharge above magnetron sputtered

targets strongly depends on orientation of magnets in individual magnetrons [81], see Fig.2. The knowledge of this fact is of key importance for a placing of the substrate on which the coating is sputtered in front of the dual magnetron.

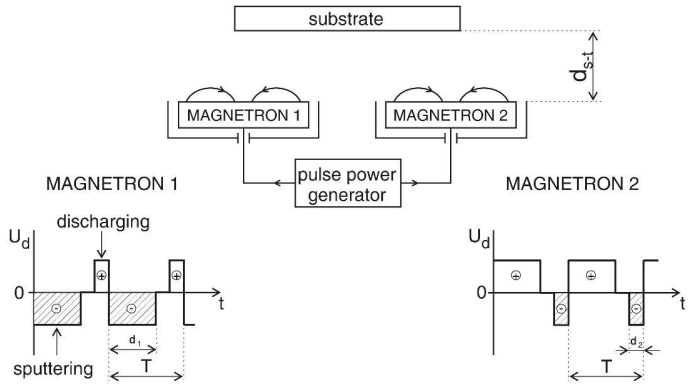

Fig. 1. Schematic diagram of symmetric bi-polar dc pulsed dual magnetron sputtering [80].

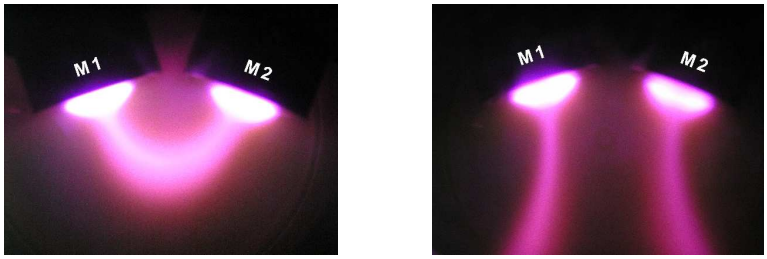

a) b)

Fig. 2. Photos of the discharge of the dual magnetron operated in a bipolar mode at repetition frequency of pulses f_r = 100 kHz, discharge current I_d = 0.5 A in nitrogen at p_{N2} = 0.5 Pa. (a) Closed magnetic **B** field and (b) Mirror magnetic **B** field [82].

The energy $\mathcal{E}$ delivered to the growing coating has a crucial effect on its structure, microstructure, elemental and phase composition, and physical properties [83-88]. The energy can be delivered by (i) the substrate heating $\mathcal{E}_{sh}$, (ii) the conversion of the kinetic energy $\mathcal{E}_p$ of bombarding ions ($\mathcal{E}_{bi}$) and fast neutrals ($\mathcal{E}_{fn}$) incident on the surface of growing film, (iii) the heat evolved during formation of the compound $\mathcal{E}_{ch}$ (the energy released in exothermic chemical reactions), (iv) the heating from the sputtered magnetron target $\mathcal{E}_{mt}$ which almost always is not perfectly cooled, and (v) the radiation from the plasma $\mathcal{E}_{rad}$. The total energy $\mathcal{E}_T$ delivered to the growing coating can be expressed by the following formula [88]

$$\mathcal{E}_T = \mathcal{E}_{sh}(T_s, t_d) + \mathcal{E}_p(U_s, i_s, a_D, p_T, t_d) + \mathcal{E}_{ch}(t_d, T_a) + \mathcal{E}_{mt}(W_d, t_d, d_{s-t}) + \mathcal{E}_{rad}(t_d) \quad (1)$$

where t_d is the time of the film deposition, T_a is the annealing temperature, $p_T = p_{Ar} + p_{RG}$ is the total pressure of sputtering gas mixture, p_{Ar} and p_{RG} are the partial pressures of argon and reactive gas (RG), respectively, $W_d = (U_d I_d)/S$ is the magnetron target power density, I_d and U_d are the magnetron current and voltage,

respectively, S is the whole area of magnetron target and d_{s-t} is the substrate-to-target distance. The energy delivered to the growing coating by incident particles $\boldsymbol{\mathcal{E}}_p$ is composed of two terms

$$\boldsymbol{\mathcal{E}}_p = \boldsymbol{\mathcal{E}}_{bi} + \boldsymbol{\mathcal{E}}_{fn} \quad (2)$$

In the simplest case of a collisionless, fully ionized plasma when $\boldsymbol{\mathcal{E}}_{fn} = 0$, the energy $\boldsymbol{\mathcal{E}}_p$ can be expressed in the following form [84-88]

$$\boldsymbol{\mathcal{E}}_p\,[J/cm^3] = \boldsymbol{\mathcal{E}}_{bi} = \boldsymbol{\mathcal{E}}_i\,(\nu_i/\nu_{ca}) = e(U_s - U_p)i_s/a_D \approx (U_s i_s)/a_D \quad (3)$$

where $\boldsymbol{\mathcal{E}}_i$ is the energy of one ion, ν_i and ν_{ca} is the flux of ions and condensing atoms, respectively, and e is the electron charge, U_s is the substrate bias, U_p is the plasma potential, i_s is the substrate ion current density and a_D is the film deposition rate.

Despite the fact that Eq.(3) is very simplified it is very useful because it can use the measured values of U_s, i_s and a_D not only to assess easily the energy $\boldsymbol{\mathcal{E}}_{bi}$ delivered to the growing coating but also to determine necessary electron density of the plasma in the magnetron discharge to reach a required value of $\boldsymbol{\mathcal{E}}_{bi}$. Moreover, this formula clearly shows a very strong effect of the deposition rate a_D on the value $\boldsymbol{\mathcal{E}}_{bi}$. This effect is very important particularly in a reactive magnetron sputtering when the deposition rate a_D decreases with increasing partial pressure of reactive gas p_{RG} at the same discharge current I_d of the magnetron discharge, see Fig.3. From this figure it is clearly seen that in formation of the stoichiometric and overstoichiometric $Ti(Fe)N_{x \geq 1}$ nitride coatings a greater energy $\boldsymbol{\mathcal{E}}_{bi}$ is delivered during their growth compared with that delivered to the substoichiometric $Ti(Fe)N_{x < 1}$; here x = N/(Ti + Fe). It is very important fact because the magnitude of the energy $\boldsymbol{\mathcal{E}}_{bi}$ decides on the microstructure and the macrostress σ generated in growing coating. More details are given below in the section 4.

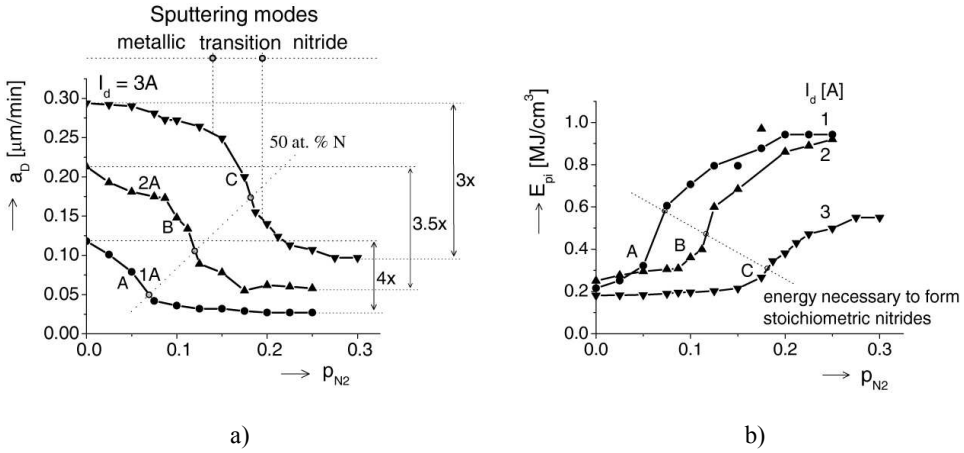

Fig.3. (a) Deposition rate a_D of $Ti(Fe)N_x$ films and (b) energy E_{bi} delivered to them during their growth by bombarding ions as a function of p_{N2}. The films were sputtered using a DC magnetron equipped with a TiFe (90/10 at.%) alloy target of 100 mm in diameter at (i) I_d = 1 A, i_s = 0.5 mAcm^{-2}, (ii) I_d = 2 A, i_s = 1 mAcm^{-2}, (iii) I_d = 3 A, i_s = 1 mAcm^{-2}, and U_s = -100 V, T_s = 300°C, d_{s-t} = 60 mm and $p_T = p_{Ar} + p_{N2}$ = 0.5 Pa [80].

The value of the $\boldsymbol{\mathcal{E}}_{bi}$ is controlled by three parameters: (1) the substrate bias U_s, (2) the substrate ion current density i_s and (3) the deposition rate of coating a_D. The substrate bias U_s is negative and should be low ($|U_s| \leq 50$ V) to avoid the generation of defects in growing coating. The substrate ion current density i_s should be greater than 1 mA/cm^3 to efficiently influence the growth mechanism of growing coating. The deposition rate a_D should be selected according to the requirement what coating – porous coating with columnar microstructure and tensile macrostress ($\sigma > 0$) or dense coating with voids-free microstructure and compressive macrostress ($\sigma < 0$) – should be formed. For the formation of porous coatings a lower energy $\boldsymbol{\mathcal{E}}_{bi}$ is sufficient. On the other hand, a higher energy $\boldsymbol{\mathcal{E}}_{bi}$ is necessary to form dense, voids-free coatings; for details see below the section 4.

The achievement of a higher energy $\mathcal{E}_{bi}$ in sputtering systems is a quite difficult problem. The magnitudes of i_s and a_D strongly depend on the discharge power P_d and the distance d_{s-t} between the substrate and the sputtered target. The energy $\mathcal{E}_{bi}$ can be increased by decreasing the deposition rate a_D. The decrease of a_D at constant P_d can be achieved by increasing d_{s-t} because $a_D \sim 1/(d_{s-t})^2$. However, increase of d_{s-t} means that the substrate is located into less intensive discharge from which lower ion current I_s can be extracted to the substrate at a given value U_s. It results in no increase but on the contrary in the decrease of the energy $\mathcal{E}_{bi}$. Therefore, it is necessary to increase the ionization of the sputtering gas. It can be achieved by an independent ionization of sputtering gas in the sputtering system. The independent ionization of sputtering gas can be realized, for instance, either using a hot cathode electron beam or hollow cathode discharge or their combination, see Fig.4. These sputtering systems are perspective for the sputtering of coatings at higher values of the energy $\mathcal{E}_{bi}$ and the formation of new advanced nanocomposite coatings. Recently, high power impulse magnetron sputtering (HIPIMS) process was developed [89-102]. In HIPIMS process when extremely high target power densities $W_t = U_d I_d / S_t$ ranging from ~100 W/cm^2 to ~ several kW/cm^2 are used at low values of the duty cycle $\tau/T \leq 0.1$ very high deposition rates a_D during pulse on time and high ionization of sputtered atoms (up to 90%) are achieved. It means that the HIPIMS process can substitute the cathodic arc evaporation process and produce coatings without macroparticles. It is main advantage of the HIPIMS process. However, the high deposition rate a_D of coating about several hundreds of nm during its growth, i.e. during the pulse on time, results in the decrease of the energy $\mathcal{E}_{bi}$ delivered by ions to growing coating. At present, the effect of the energy $\mathcal{E}_{bi}$ on properties of coatings produced by the HIPIMS process is not still understood well and thus it is intensively investigated in many laboratories worldwide. For the low-temperature ($T_s \leq 100$°C) sputtering of nanocomposite coatings new magnetrons operating at low pressures $p \leq 0.1$ Pa of sputtering gas are necessary to be developed [74]. These examples clearly show that for the creation of the advanced nanocomposite coatings with new unique properties new magnetrons and sputtering systems need to be developed.

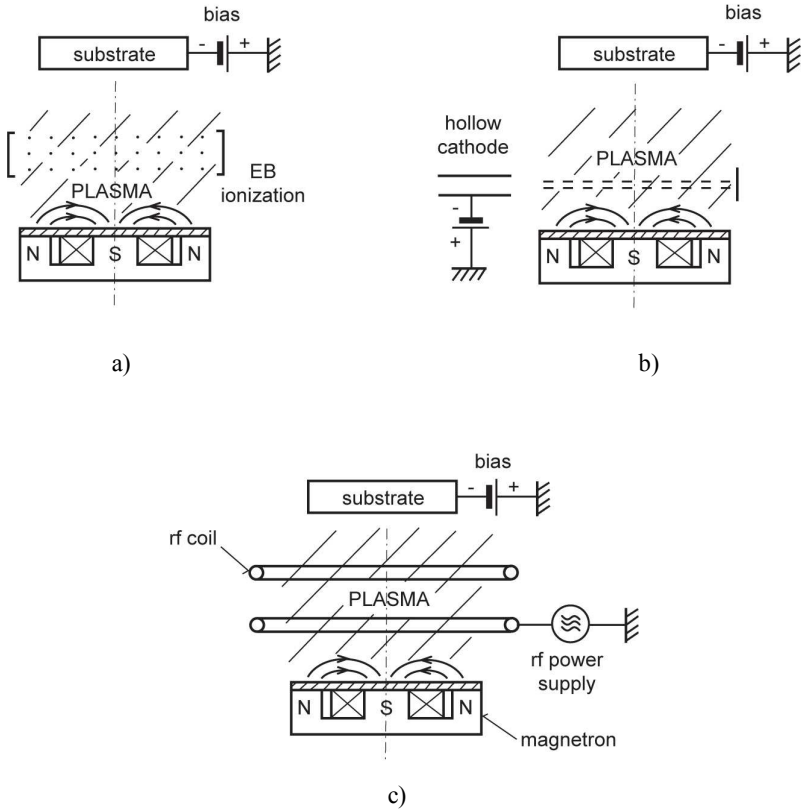

Fig.4. Magnetron with additional ionization of sputtering gas using a) the electron beam, b) the hollow cathode discharge and c) the inductively coupled RF discharge. Adapted after Ref. [80].

3. Flexible hard nanocomposite coatings and their main characteristics

The principle of formation of the flexible hard coatings can be explained with the aid of the Hooke's law

$$\sigma = \varepsilon.E \quad (4)$$

where σ is the stress (load), ε is the strain (deformation) and E is the Young's modulus. If we need to form the material which allows a high elastic deformation prior to a failure, i.e. the material with a high value ε at a given value of stress σ, its Young's modulus E must be reduced. It means that the materials with the lowest value of the Young's modulus E at a given hardness H (σ = const) need to be developed. It is a simple solution but a quite difficult task. A possible behaviour of the material can be best illustrated in the stress σ vs. strain plane. The stress σ vs the strain ε dependences for brittle, tough, resilient and ductile hard coatings are schematically displayed in Fig.5.

Superhard materials are very brittle, exhibit almost no plastic deformation and a very low strain at failure $\varepsilon = \varepsilon_1$. Hard and tough materials exhibit both the elastic and plastic deformation. The material withstanding a higher strain $\varepsilon_1 << \varepsilon \leq \varepsilon_{max}$ without cracking exhibits a higher toughness. The hardness of tough materials is higher in the case when a greater value of ε_{max} is achieved at higher values of σ_{max}. Such materials exhibit a high strength. On the contrary, the materials with $\sigma < \sigma_{max}$ and $\varepsilon_{\sigma max} < \varepsilon < \varepsilon_3$ are ductile, exhibit a lower strength and a high ductility. Hard and tough materials with no plastic deformation (blue line 0A) are the resilient hard coatings with 100% elastic recovery W_e. The hardness H of hard, tough and highly elastic coatings, ranging from about 15 to 25 GPa, is, however, sufficient for many applications. The main advantage of the highly elastic (flexible) coatings with a low plastic deformation is their enhanced resistance to cracking. These are reasons, why the hard, tough and flexible hard coatings are now intensively developed in many labs worldwide. The hard and simultaneously tough and flexible coatings represent a new generation of advanced hard nanocomposite coatings.

The analysis given above shows that a new task in the development of advanced hard flexible nanocomposite coatings with enhanced toughness is to master the formation of coatings with (i) the low value of the effective Young's modulus E^* and (ii) a high value of the elastic recovery W_e. The hard flexible coatings with enhanced toughness, low values of E^* and high values of W_e were already prepared by magnetron sputtering [41,44-52]. Also, it was found that these hard nanocomposite coatings with enhanced toughness exhibit (i) the enhanced resistance to cracking and (ii) the high ratio $H/E^* \geq 0.1$ and (iii) the high elastic recovery $W_e \geq 60\%$. More details are given below and in the reference [41].

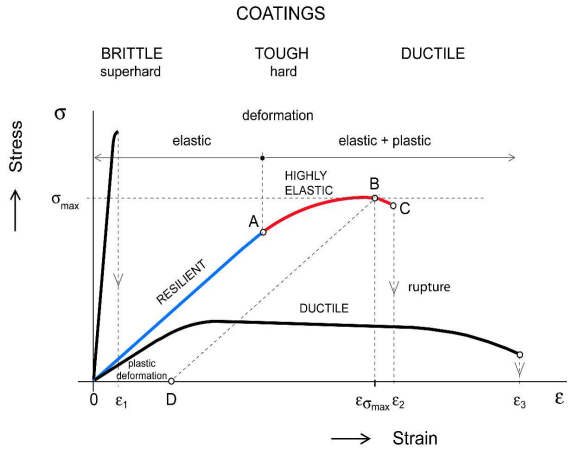

Fig.5. Schematic illustration of stress σ vs strain ε curves of super-hard (brittle), hard (tough), hard (resilient) and ductile coatings. Resilient coatings exhibit no plastic deformation (line 0A). Adapted from Ref. [41].

4. Design of flexible hard nanocomposite coatings

During many investigations of the interrelationships between the deposition parameters of coatings and their properties the general rules enabling to design the hard coatings resistant to cracking were discovered. It was found that these coatings should exhibit simultaneously the following properties [41,44]

1. The low effective Young's modulus E^* resulting in a high ratio $H/E^* \geq 0.1$ and the high elastic recovery $W_e \geq 60\%$
2. The dense, voids-free microstructure.
3. The compressive macrostress ($\sigma < 0$)

All these properties (H, E^*, W_e, H/E^* ratio, microstructure, macrostress σ, elemental and phase composition) of hard coatings resistant to cracking are controlled by (1) the energy $\boldsymbol{\varepsilon}_p = \boldsymbol{\varepsilon}_{ca} + \boldsymbol{\varepsilon}_{bi}$ delivered to the growing coating by condensing atoms ($\boldsymbol{\varepsilon}_{ca}$) and bombarding ions ($\boldsymbol{\varepsilon}_{bi}$) and the substrate heating (T_s) and (2) the kind and the amount of elements added in the base material of coating what moreover decides also on the value of the melting temperature T_m of the coating material. The relationships between the energy $\boldsymbol{\varepsilon}_{bi}$, the microstructure of coating, the macrostress σ generated in growing coating and the melting temperature T_m of the coating material are clearly illustrated in Figs. 6 and 7.

Fig.6 shows the evolution of the film microstructure in 3D representation as a function of the T_s/T_m ratio (the equilibrium heating of substrate) and the sputtering pressure of argon p_{Ar}, i.e. as a function of *the energy* $\boldsymbol{\varepsilon}_p$ *delivered to the growing film by incident condensing of neutral particles* (non-equilibrium heating). The evolution of the film microstructure displayed in Fig.6 is called the structural zone model (SZM). The SZM of the sputtered metallic films was developed by J.A.Thornton in 1977 [104]. The SZM is divided in four zones: (1) the zone 1 composed of tapered crystallites separated by voids, (2) the zone T composed of fibrous grains embedded in a voids-free amorphous matrix, (3) the zone 2 composed of columnar grains separated by dense inter-crystalline boundaries [105] and (4) the zone 3 composed of recrystallized grain structure. The boundary between the zone 1 and the zone T corresponds to zero macrostress $\sigma = 0$ generated in sputtered films and separates the films with a low-density microstructure composed of columns separated by voids (the zone 1) from the films with a dense, voids-free microstructure composed of fibrous grains embedded in an amorphous inter-grain phase (the zone T). Very different microstructure in the zone 1 and the zone T is a main reason why properties of the films formed in the zone 1 and the zone T so strongly differ and why the films formed in the zone T exhibit unique properties.

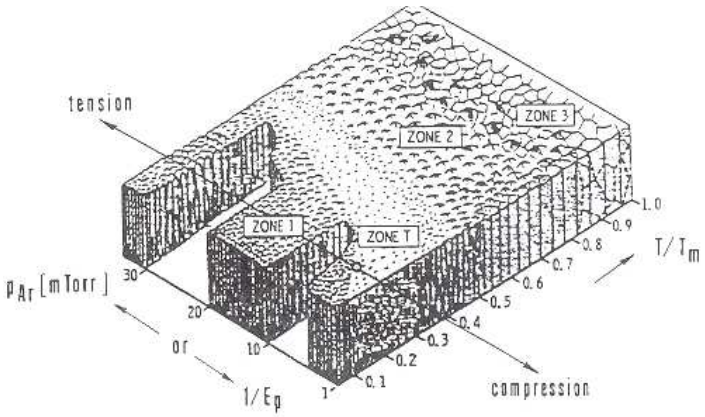

Fig.6. Structural zone model (SZM) of sputtered metallic films developed by J.A.Thornton. Adapted after Ref. [104].

Fig.7 shows the macrostress σ as a function of the energy $\boldsymbol{\varepsilon}_{bi}$. The effect of the melting temperature T_m of film material on the magnitude and kind of macrostress σ and on the microstructure of film are also clearly seen in this figure. The macrostress σ generated in the growing film also very well correlates with its microstructure; see Fig.6 and photos inserted in Fig.7. From Fig.7 four general and very important issues can be drawn

1. The macrostress σ changes from tensile ($\sigma > 0$) to compressive ($\sigma < 0$) with increasing energy $\boldsymbol{\varepsilon}_{bi}$

2. There is a critical value of $\mathcal{E}_{bi} = \mathcal{E}_c$ at which films exhibit zero macrostress $\sigma = 0$.
3. The values of the macrostress σ and the critical energy $\mathcal{E}_c$ depend on the melting temperature T_m of the film material.
4. The macrostress σ and the critical energy $\mathcal{E}_c$ increase with increasing T_m of coating material.

The magnitude of the critical energy $\mathcal{E}_c$ depends on (i) the substrate bias U_s and the substrate ion current density i_s, (ii) the deposition rate a_D of film, (iii) the sputtering gas pressure p, (iv) the substrate temperature T_s, (v) the kind and amount of the element added in the film what determines the melting temperature T_m of the film material, and (vi) the contamination of film by oxygen O and nitrogen N from a residual atmosphere in the deposition chamber when the film is deposited at low deposition rates a_D [107], i.e. that the critical energy E_c = f(E_{bi}, elemental composition, T_m, p, p_0) is a very complex function depending on many deposition and film material parameters; here p is the sputtering gas pressure and p_0 is the base pressure in deposition chamber.

Many experiments performed so far show that the films formed in the zone T exhibit not only dense, voids-free microstructure composed of tiny fibrous grains embedded in an amorphous matrix and compressive macrostress $\sigma < 0$ but also a high ratio $H/E^* \geq 0.1$ and high values of the elastic recovery $W_e \geq 60\%$. It means that films formed in the zone T can be flexible and thereby automatically can exhibit an enhanced resistance to cracking if the sufficient energy $\mathcal{E} > \mathcal{E}_c$ is delivered in films during their growth. Three examples of flexible films are given below in the section 5, 6 and 7.

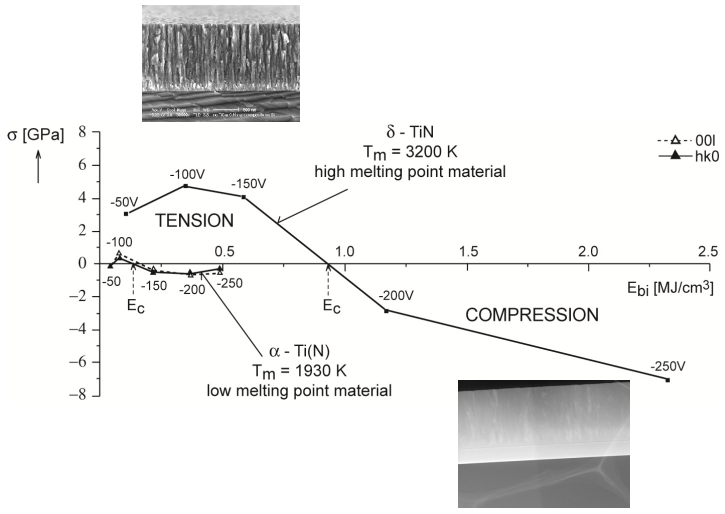

Fig. 7. Macrostress σ in sputtered α - Ti (N) and δ - $TiN_{x \approx 1}$ films as a function of energy $E_{bi} = U_s i_s / a_D$ delivered to them by bombarding ions at $p_T = p_{Ar} + p_{N2} = 5$ Pa and $T_s = 350°C$, i.e. at $T_s/T_m = 0.32$ and 0.19 for the α - Ti(N) film and the δ - $TiN_{x \approx 1}$film , respectively. Adapted after Ref. [24,106].

In summary, it can be concluded that *the formation of films with microstructure corresponding to the zone T of the Thornton's SZM requires deliver to films during their growth a sufficiently high energy $\mathcal{E}$, which must exceed the critical energy $\mathcal{E}_c$.*

5. Flexible protective coatings

In many cases, the surface of materials needs to be protected against damage, for instance, scratching, oxidation, corrosion, erosion, etc. In these cases protective coatings are used. Such coatings have to be simultaneously hard and flexible, and particularly when they are deposited on flexible substrates they must exhibit an enhanced resistance to cracking during the substrate bending. Such the properties exhibit flexible hard films described above.

The resistance of the protective flexible coating to cracking is demonstrated in the Zr-Al-O system. In this system the flexibility of coating and its resistance to cracking is controlled by the Zr/Al ratio, i.e. by the elemental composition of coating. The Zr/Al ratio strongly influences the mechanical properties of the Zr-Al-O coating and thereby its resistance to cracking. The Zr-Al-O coatings with a low ratio Zr/Al < 1 exhibit a low ratio $H/E^* < 0.1$ and a low elastic recovery $W_e < 60$ %, are brittle and easily crack in bending. On the contrary, the Zr-Al-O coatings with a high ratio Zr/Al > 1 exhibit a high ratio $H/E^* \geq 0.1$ and a high elastic recovery $W_e \geq 60$ %, are flexible and well resists to cracking in bending. This fact is illustrated in Fig.8. More detail is given in Ref. [46,48].

Recently, the resistance of the film against cracking was demonstrated also in the following coating systems: (1) Al-Cu-O oxide/oxide nanocomposite coating [45], (2) Zr – Al – O oxide/oxide nanocomposite coating [46,48], (3) Al-O-N nitride/oxide nanocomposite coating [47], (4) Si – Zr – O oxide/oxide nanocomposite coating [49], (5) Ti-Ni-N nitride/nitride nanocomposite coating [50], (6) Al-Cu-N nitride/nitride nanocomposite coating [51] and (7) $(Ti,Al,V)N_x$ nitride/nitride nanocomposite coating [52]. All these coatings exhibit the high ratio $H/E^* \geq 0.1$ and high elastic recovery $W_e \geq 60\%$. This finding clearly indicates that the high ratio $H/E^* \geq 0.1$ and high $W_e \geq 60\%$ are key parameters necessary for the formation hard films resistant to cracking. For more details see the papers [45-52].

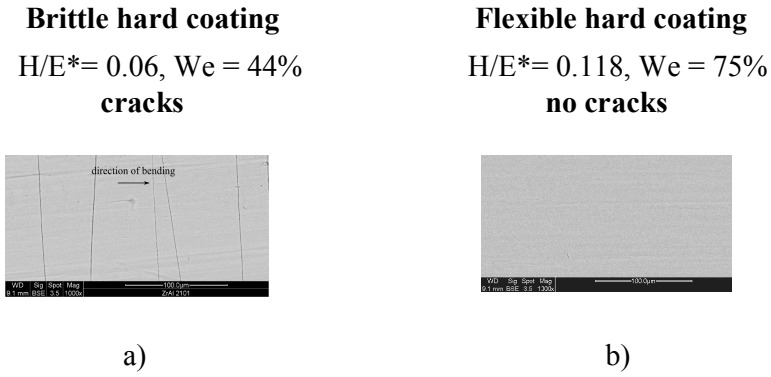

Fig.8. Comparison of surface morphology of (a) brittle and (b) flexible ~3000 nm thick Zr-Al-O coating reactively sputtered at $U_s = U_{fl}$, $T_s = 500°C$ and $p_T = 1$ Pa on Mo strip after bending around steel cylinder of radius r = 12.5 mm [44,48].

6. Flexible functional coatings

Many functional coatings are brittle, easily crack and thus they lose its function during the operation. Therefore, it is vitally important to develop flexible functional coatings with an enhanced resistance to cracking. The possibility to form functional coatings resistant to cracking is demonstrated in two systems Cr-Cu-O [103] and Al-Cu-N [51] of antibacterial coatings with different elemental composition. The Cu content in the coating decides on its antibacterial function, i.e. on the efficiency of the killing of bacteria on the coating surface. The efficiency of killing of bacteria increases with increasing Cu content in the coating, see Fig.9.

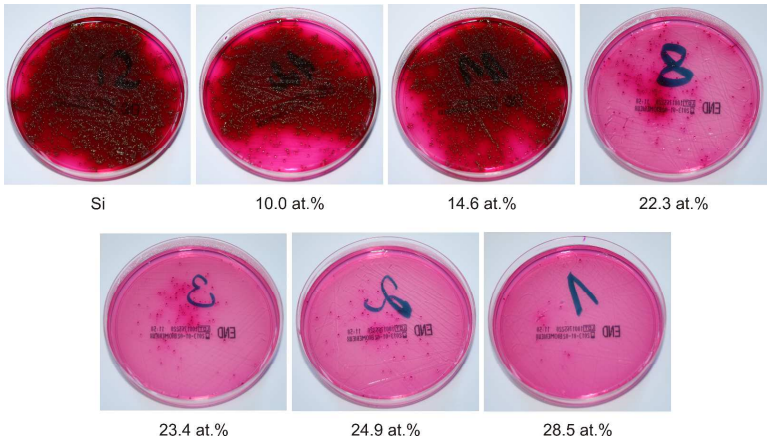

Fig.9. Photos of Petri dishes with Endo agar and colonies of *Escheria coli* bacteria cultivated from bacterial suspensions which were in contact with a-(Cr-Cu-O) coatings with various at.% of Cu in the dark for 5 hours. The films were sputtered on Si(100) substrate at floating potential (U_s=U_{fl}) and T_s=500°C [103]. Dark areas in this figure are colonies of living *Escheria coli* bacteria.

From Fig.9 it is seen that a high amount of Cu of about 20 at.% in the Cr-Cu-O coatings is necessary to kill all bacteria on the coating surface. However, such high content of Cu in the coating results in low values of H, E^*, W_e and H/E^* ratio, see Table 1. It means that the Cr-Cu-O film with ~ 20 at.% Cu exhibits a low mechanical protection against fretting and cracking in bending, particularly in the case when the coating is deposited on a flexible substrate. This coating exhibits 100% efficiency of killing of E.coli bacteria, see Fig.9 but very easily cracks, see Fig.10 and Table 1. Therefore, it was highly desirable to develop an antibacterial coating which simultaneously efficiently kills bacteria on its surface and exhibits an enhanced resistance against mechanical damages and cracking. It was found that the Cr-Cu-N coating perfectly fulfils both requirements. The replacement of O by N makes it possible (i) to reduce Cu content from ~20 at.% to ~10 at.% for 100% killing of all *E.coli* bacteria and (ii) to increase the hardness H from ~ 3 GPa to ~ 20 GPa, the elastic recovery W_e from 36 to 74%, H/E^* ratio from 0.046 to 0.122, and to convert the macrostress σ from tensile to compressive (σ < 0), i.e. to reach conditions which are necessary to produce highly flexible antibacterial coating with enhanced resistance to cracking in bending. The enhanced resistance of the Cr-Cu-N antibacterial coating to cracking was confirmed by its deposition on Mo strip (55 x 9 x 0.15 mm^3) and bending around a fixed cylinder of radius r = 10 mm, see Fig.10. It means that while the Cr-Cu-O coating is one-functional antibacterial coating, the Al-Cu-N coating is two-functional antibacterial/flexible coating.

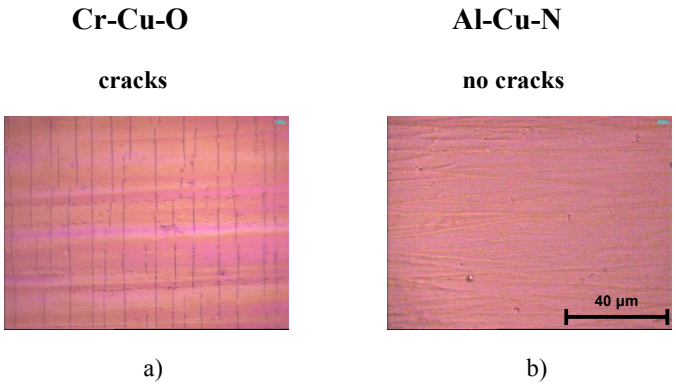

Fig.10. Surface morphology of (a) Cr-Cu-O oxide coating with H/E^*< 0.1 and (b) Al-Cu-N coating with H/E^*> 0.1 deposited on Mo strip (55 x 15 x 0.15 mm^3) after bending around cylinder of radius r = 10 mm, respectively [44,52].

At present, one of the hottest tasks is, for instance, to develop and master the production of three-functional flexible/transparent/electrically conductive coatings.

Table 1. Thickness h, deposition rate a_D, deposition parameters, physical and mechanical properties of sputtered Cr-Cu-O and Al-Cu-N coatings and the assessment of their resistance to cracking by bending illustrating in Fig.10.

Coating	h [nm]	a_D [nm/min]	T_s [°C]	U_{sp} [V]	i_{sp} [mA/cm^2]	σ [GPa]	Cu [at.%]	H [GPa]	E^* [GPa]	W_e [%]	H/E^*	cracks bending
Cr-Cu-O	2190	18.3	500	U_{fl}	-	0.1	19.5	3.2	70	36	0.046	yes
Al-Cu-N	2730	63.5	400	-100	1.38	-1.7	9.6	21.9	180	74	0.122	no

Here, i_{sp} is the averaged substrate ion current density over negative pulse of substrate bias U_{sp} [44, 52,103].

In summary it is necessary to conclude that the formation of two- and multi-functional coatings with maximally optimized functions is quite difficult but possible process. The formation of such films is controlled by a combined action of the elemental composition of coating and the energy $\mathcal{E}$ delivered to the growing coating [41,44].

7. Flexible over-layer preventing cracking of brittle coatings

Sometimes it is impossible to form flexible functional coatings because these coatings are brittle. Therefore, it is important to find a way how to prevent cracking of the brittle coatings. The principle preventing the brittle coatings from cracking is based on over-coating of the brittle coating by the elastic over-layer with high ratio $H/E^* \geq 0.1$, high elastic recovery $We \geq 60\%$ and compressive macrostress $\sigma < 0$ [49].

The experimental evidence of the validity of this principle is illustrated in Fig.11. This figure shows the surface morphology of (a) the single-layer brittle Zr-Si-O coating with low ratio $H/E^* = 0.08$, low elastic recovery $We = 50\%$ and tensile macrostress $\sigma = 0.25$ GPa and (b) the two-layer coating composed of the same brittle Zr-Si-O coating (the bottom layer) and the elastic Zr-Si-O film with high ratio $H/E^* = 0.1$, high elastic recovery $We = 68\%$ and compressive macrostress $\sigma = -1.5$ GPa (the top layer) sputtered on a Mo strip (60 x 10 x 0.1 mm^3) after bending of the coated strip around the cylinder with diameter of r = 12.5 mm. As expected, the single-layer coating with the low ratio $H/E^* < 0.1$, low elastic recovery $We < 60\%$ and tensile macrostress $\sigma > 0$ easily cracks in bending around the cylinder of radius r = 12.5 mm already at a small bending angle $\alpha \approx 30°$, see Fig.11a. On the contrary, the two-layer coating in which the same layer 1 as in the single-layer coating is covered by the layer 2 with high ratio $H/E^* \approx 0.1$, high elastic recovery $We > 60\%$ and compressive macrostress $\sigma < 0$ exhibits no cracks even after bending up to angle $\alpha=180°$ around the cylinder with the same radius r = 12.5 mm, see Fig.11b.

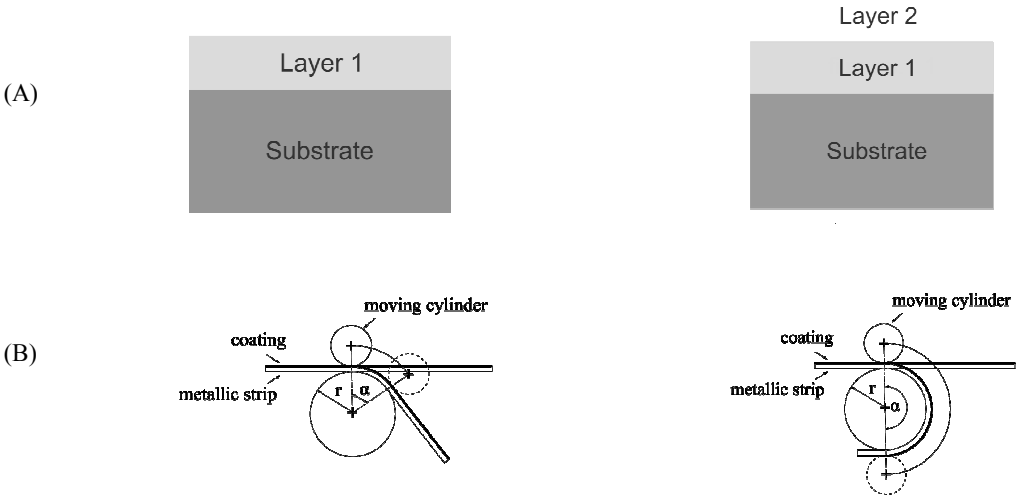

(C)

a) b)

Fig.11. Schematic illustration of (A) coating/substrate geometry, (B) method of bending of the coated Mo strip and (C) photos of surface morphology of (a) single-layer Zr-Si-O coating with low ratio H/E*< 0.1, low elastic recovery We < 60% and tensile macrostress $\sigma > 0$ (the layer 1) and (b) two-layer Zr-Si-O coating composed of the bottom layer with low ratio H/E*< 0.1, low elastic recovery We < 60% and tensile macrostress $\sigma > 0$ (the layer 1) and the upper layer with high ratio H/E* ≥ 0.1, high elastic recovery We > 60% and compressive macrostress $\sigma < 0$ (the layer 2) after bending around the cylinder with diameter of r = 12.5 mm [49].

This experiment clearly demonstrates that the brittle coating can be protected against cracking by the highly elastic over-layer with high ratio H/E* ≥ 0.1, high elastic recovery We ≥ 60% and compressive macrostress $\sigma < 0$. Here, it is worthwhile to note that the compressive macrostress ($\sigma < 0$) of the elastic over-layer plays a very important role preventing the brittle coating (the layer 1) from cracking. However, more experiments are needed to be done to find the best way how to reach a maximal resistance of the brittle coating to cracking.

8. Flexible multilayer coatings resistant to cracking

Recent experiments indicate that the alternation of the macrostress σ in multi-layered coatings could be a new approach in formation of very thick (≥ 10 μm) coatings with enhanced resistance to cracking. This hypothesis was tested in three-layer and four-layer Zr-Si-O coatings composed of alternating layers in tension ($\sigma > 0$) and compression ($\sigma < 0$) sputtered on a Mo strip (60 x 10 x 0.1 mm^3). The surface morphology of these Zr-Si-O coatings together with the one-layer and two-layer Zr-Si-O coatings after bending around the fixed cylinder of radius r =12.5 mm is shown in Fig.12. The layer in tension is denoted as the layer 1 (L1) and the layer in compression is denoted as the layer 2 (L2). The first layer deposited at the substrate was always the layer 1. The thicknesses h_n of individual layers in the coating and its mechanical properties are given in Table 2; the index n denotes the number of layer in the coating.

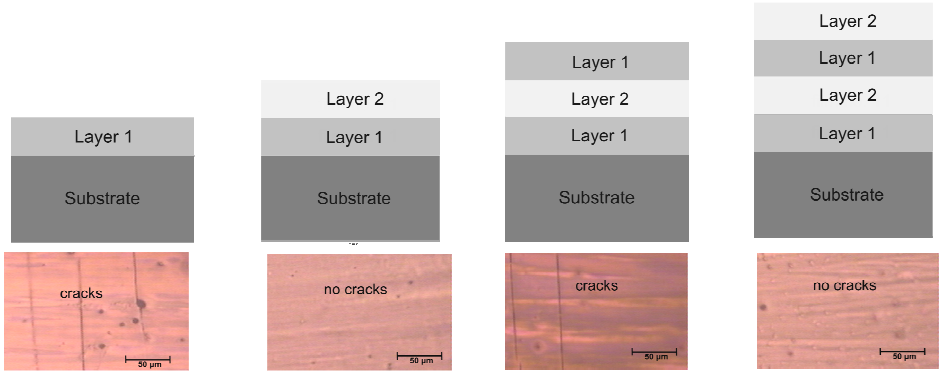

a) b) c) d)

Fig.12. Surface morphology of (a) one-layer, (b) two-layer, (c) three-layer and (d) four-layer Zr-Si-O coating deposited on Mo strip after bending around fixed cylinder of radius r = 12.5 mm [49].

Table 2. Thickness h_n of individual layers in the multilayer Zr-Si-O coatings, their mechanical properties, macrostress σ in the top layer, and cracks created in multilayer coating during bending of coated Mo strip around fixed cylinder of radius r = 12.5 mm [49].

Coating	content of layers	h_1 [nm]	h_2 [nm]	h_3 [nm]	h_4 [nm]	h_T [nm]	H [Gpa]	E^* [Gpa]	W_e [%]	H/E^*	macrostress in top layer	cracks in bending
Coating A	L_1	3000	-	-	-	3000	12.6	161	50	0.078	tension	yes
Coating B	L_1+L_2	3000	3000	-	-	6000	17.6	165	70	0.107	compression	no
Coating C	$L_1+L_2+L_3$	2500	2500	2500	-	7500	12.2	149	56	0.082	tension	yes
Coating D	$L_1+L_2+L_3+L_4$	2400	2400	2400	2400	9600	16.6	157	70	0.106	compression	no

From Fig.12 it is seen that the alternation of the layers in tension and compression strongly influences the resistance of the coating to cracking. Always, when the top layer is in tension ($\sigma > 0$) the coating cracks. On the contrary, when the top layer is in compression ($\sigma < 0$) the coating does not cracks, i.e. the coating exhibits an enhanced resistance to cracking. This is a very important phenomenon which can be used in the formation of new advanced very thick (10 to 100 μm) coatings. Also, it is worthwhile to note that the layer 1 is X-ray amorphous and the layer 2 is crystalline; more details are in Ref. [44,49]. Based on this experiment new very thick multilayer coatings composed of many crystalline/X-ray amorphous bi-layers can be realized, see Fig.13. At present, such thick multilayer coatings are under investigation in our labs. Moreover, it can be expected, that these coatings will exhibit new unique properties.

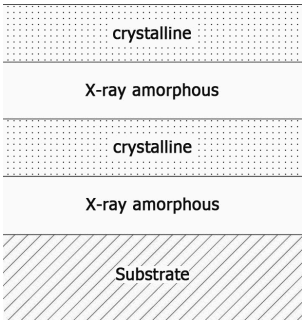

Fig.13. Multilayer coating composed of alternating X-ray amorphous and crystalline layers.

However, many questions still remain open. For instance, what is a minimum thickness of the layer in compression which is sufficient to prevent the cracking of the multilayer coating, what is the effect of layers with alternating macrostress σ on physical properties of the multilayer coating, what is the thermal stability and the thermal conductivity of the multilayer coating composed of layers with macrostress σ alternating from tension ($\sigma > 0$) to compression ($\sigma < 0$), what should be the structure and the microstructure of the layer on the substrate/coating interface to achieve maximum adhesion of the coating to the substrate, etc. These tasks are a subject of our next investigation.

9. Low-temperature sputtering of flexible nanocomposite coatings

In the section 4 above, it was shown that the flexible films can be formed in the zone T of the SZM. However, to form coatings in the zone T it is necessary to overpass the boundary line between the zone 1 and the zone T, which in the 2D representation of the SZM is a function of the ratio T_s/T_m and the sputtering gas pressure p, see Fig.14. Therefore, it is important to show, how the location of the boundary line between the zone 1 and zone T can be controlled. The principle of the low-temperature sputtering of films with microstructure of zone T is based on replacement of the equilibrium substrate heating (T_s) by the non-equilibrium atomic scale heating (ASH) [41,44,74].

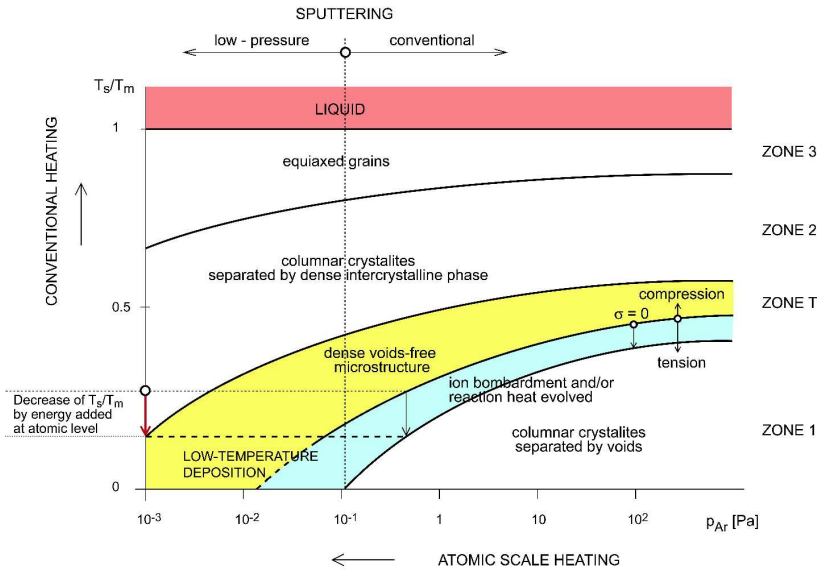

Fig.14. Thornton's structural zone model (SZM) of sputtered films extended to the region of low sputtering gas pressures. Adapted after Ref. [74].

The location of the boundary line between the zone 1 and the zone T in the SZM can be influenced by (1) the energy $\mathcal{E}_{bi}$ delivered to the growing film by bombarding ions when the films are formed at negative substrate bias $U_s < 0$ [108,109] and (2) by the energy $\mathcal{E}_{fn}$ delivered to the growing film by fast neutral particles controlled by the pressure p of sputtering gas and increasing with decreasing p. The boundary line between the zone 1 and the zone T shifts to lower values of the ratio T_s/T_m with increasing negative substrate bias U_s and decreasing sputtering gas pressure p, see Fig.14. It means that the films with the microstructure of the zone T can be formed at low values T_s/T_m, i.e. at low substrate temperatures T_s, even at unheated substrates (T_s = RT). Here, it is important to underline that the deposition of the films with microstructure corresponding to the zone T of the Thornton's SZM at low values of T_s/T_m ratio is possible also without using a negative substrate bias U_s, i.e. at the substrate held at the floating potential ($U_s = U_{fl}$), when the films are sputtered at low pressures p, see Fig.14. However, new low-pressure magnetrons need to be developed for the formation of films at very low pressures p. More details are given in Ref. [42,61,74,80].

The possibility to form the films with the microstructure corresponding to the zone T of the Thornton's SZM at low substrate temperatures $T_s \leq 100°$ C is of a great potential for many advanced applications, namely for flexible electronics, flat panel displays, MEMS systems, formation of functional films on polymer foils and fabrics, etc. The formation of nanocrystalline or even crystalline films with the microstructure corresponding to the zone T at low substrate temperatures $T_s \leq 100°$C can be realized also by the addition of selected elements in the film because the melting temperature T_m of such films can be decreased compared to the pure films and thereby the T_s/T_m ratio can be increased.

In summary it can be concluded that the films with dense, voids-free microstructure, compressive macrostress $\sigma < 0$ and enhanced resistance to cracking can be formed in the zone T of the Thornton's SZM also at low substrate temperatures $T_s \leq 100°$C, i.e. at low values of T_s/T_m ratio, when sufficient energy $\mathcal{E}_{bi}$ is delivered to the growing film by bombarding ions and/or when a low sputtering gas pressure p is used. Very important role in the low-temperature sputtering of the flexible films plays also the melting temperature T_m of the film material which (i) decides on the value of T_s/T_m ratio and (ii) can be controlled by the addition of selected elements in the film.

10. Conclusions

Up to now, four important milestones have been achieved in development of the hard nanocomposite coatings: (1) the hard/hard two-phase nanocomposites with enhanced hardness H composed of two hard phases, (2) the

hard/soft nanocomposites with enhanced hardness H composed of one hard and one soft phase, (3) X-ray hard nanocomposites with high thermal stability and oxidation resistance up to ~ 1500 °C and (4) flexible hard nanocomposite coatings with high toughness and enhanced resistance to cracking. The principle of formation of the flexible hard nanocomposite coatings and several applications are reported in this article. However, there are further tasks which have to be mastered in the development of new advanced hard nanocomposite coatings. These tasks can be briefly summarized as follows

1. The low-temperature sputtering of flexible, hard, two- and multi-functional nanostructured and nanocomposite coatings.
2. The form single-phase crystalline coatings thermally stable in a wide range of temperatures from the room temperature up to very high temperatures approaching the melting temperature T_m of the coating material.
3. The detailed investigations of interrelationships between the coating properties and the energy $\mathcal{E}$ delivered to the coating during its growth or in a post-deposition treatment process.
4. The development of new deposition systems operating under new physical conditions.

There is no doubt that every even a small progress in the solution of these tasks will strongly contribute to deepen our knowledge in the field of advanced hard nanocomposite coatings and will represent a huge potential for realization of new advanced applications.

Acknowledgments

This work was supported in part by the Grant Agency of the Czech Republic under project No. P108/12/0393.

References

[1] H.Gleiter, Nanocrystalline materials, Progress in Materials Science 33 (1989), 223-315.
[2] R.Birringer, Nanocrystalline materials, Mater.Sci.Eng. A 117 (1989), 33-43.
[3] R.W.Siegel: Cluster-assembled nanophase materials, Annu.Rev.Mater.Sci. 21 (1991), 559-579.
[4] R.W.Siegel: What do we really know about the atomic-scale structures of nanophase materials?, J. Phys. Chem. Solids 55 (10) (1994), 1097-1106.
[5] R.W.Siegel and G.E.Fougere: Grain size dependent mechanical properties in nanophase materials, in Proc. Mater. Res. Soc. Symp. Vol. 362, Grant H.J., Armstrong R.W., Otooni M.A. and Ishizaki K. (Eds.), Warrendale, PA, 1995, pp.219-229.
[6] S.Vepřek and S.Reiprich: A concept for the design of novel superhard coatings, Thin Solid Films 265 (1995), 64-71.
[7] H.Gleiter: Nanostructured materials: State of the art and perspectives, Nanostructured Materials 6 (1996), 3-14.
[8] S.Yip: The strongest size, Nature 391 (1998), 532.
[9] A.A.Voevodin and J.S.Zabinski: Superhard, functionally gradient, nanolayered and nanocomposite diamond-like carbon coatings for wear protection, Diamond and Related Materials 7 (1998), 463-467.
[10] J.Musil: Hard and superhard nanocomposite coatings, Surf.Coat.Technol. 125 (2000), 322-330.
[11] H.Gleiter: Nanostructured materials: Basic concepts and microstructure, Acta Mater. 48 (2000), 1-29.
[12] A.Leyland, A.Matthews: On the significance of the H/E ratio in wear control: a nanocomposite coating approach to optimised tribological behaviour, Wear 246 (2000), 1-11.
[13] L.Hultman: Thermal stability of nitride thin films, *Vacuum* 57(1) (2000), 1-30.
[14] R.Hauert, J.Patscheider: From alloying to nanocomposites – Improved performance of hard coatings, Adv. Mater. 2(5) (2000) 247-259.
[15] S.Vepřek: Nanostructured superhard materials: Chapter 4 in *Handbook of Ceramic Hard Materials*, R.Riedel (ed.), WILEY-VCH, Weinheim, 2000, pp. 104-139.
[16] R.Hauert, J.Patscheider: From alloying to nanocomposites – Improved performance of hard coatings, Adv. Mater. 2(5) (2000) 247-259.
[17] H.Gleiter: Tuning the electronic structure of solids by means of nanometer-sized microstructures, Scripta Mater. 44 (2001), 1161-1168.
[18] R.A.Andrievskii: Thermal stability of nanomaterials, Russian Chemical Reviews, 71(10) (2002), 853-866.
[19] G.M.Demyashev, A.L.Taube and E.E.Siores: Superhard nanocomposite coatings, in *Handbook of Organic-Inorganic Hybrid Materials and Nanocomposite*, Vol. 1, H.S. Nalwa (Ed.), American Scientifuc Publishers, 2003, pp.1- 61.
[20] J.Patscheider: Nanocomposite hard coatings for wear protection, MRS Bulletin 28(3) (2003), 180-183.

[21] S.Zhang, D.Sun, Y.Fu and H.Du: Recent advances of superhard nanocomposite coatings: a review, Surf.Coat. Technol. 167 (2003), 113-119.
[22] R.A.Andrievski: Nanomaterials based on high-melting carbides, nitrides and borides, Russian Chemical Reviews, 74(12) (2005), 1061-1072.
[23] S.Zhang, D.Sun, Y.Fu and H.Du: Toughening of hard nanostructured thin films: a critical review, Surf.Coat. Technol. 198 (2005), 2-8.
[24] J.Musil: Physical and mechanical properties of hard nanocomposite films prepared by reactive magnetron sputtering, Chapter 10 in *Nanostructured Coatings,* J.T.M. DeHosson and A. Cavaleiro (Eds.) New York, Springer Science + Business Media, LCC, 2006, pp. 407-463.
[25] L.Hultman and C.Mitterer: Thermal stability of advanced nanostructured wear-resistnt coatings, Chapter 11 in *Nanostructured Coatings,* J.T.M.DeHosson and A. Cavaleiro (Eds.) New York, Springer Science + Business Media, 2006, pp. 464-510.
[26] P.H.Mayrhofer, C.Mitterer and L.Hultman: Microstructural design of hard coatings, Progress in Materials Science 51 (2006), 1032-1114.
[27] C.Lu, Y.W.Mai and Y.G.Shen: Recent advances on understanding the origin of superhardness in nanocomposite coatings: A critical review, J.Mater.Sci. 41 (2006), 937-950.
[28] C.S.Sandu, F.Medjani, R.Sanjines, A.Karimi, F.Levy: Structure, morphology and electrical properties of sputtered Zr-Si-N thin films: From solid solution to nanocomposite, Surf.Coat.Technol. 201 (2006) 4219-4229.
[29] Y.H.Lu, Y.G.Shen: Nanostructure transition: From solid solution Ti(N,C) to nanocomposite nc-Ti(N,C)/a-(C,CN_x), Appl.Phys.Lett. 90 (2007) 221913.
[30] C.S.Sandu, F.Medjani, R.Sanjines: Optical and electrical properties of Zr-Si-N thin films: From solid solution to nanocomposite, Rev. Adv. Mater. Sci. 15 (2007) 173-178.
[31] J.Musil and M.Jirout: Toughness of hard nanostructured ceramic thin films, Surf.Coat.Technol. 201 (2007), 5148-5152.
[32] A.Raveh, I.Zukerman, R.Shneck, R.Avni and I.Fried: Thermal stability of nanostructured superhard coatings: A review, Surf.Coat.Technol. 201 (2007), 6136-6142.
[33] J.Musil: Properties of hard nanocomposite thin films, Chapter 5 in *Nanocomposite films and coatings*, London, S.Zhang and N.Ali (Eds.), London, Imperial College Press, 2007, pp. 281-328.
[34] J.Musil, J.Vlcek, P.Zeman: Advanced amorphous non-oxide coatings with oxidation resistance above 1000°C, Special Issue on Nanoceramics, Advances in Applied Ceramics 107(3) (2008), 148-154.
[35] J.Musil, P.Baroch and P.Zeman: Hard nanocomposite coatings. Present status and trends, Chapter 1 in *Plasma Surface Engineering Research and its Practical Applications*, R.Wei (Ed.), Kerala, Research Signpost, 2008, pp. 1-34.
[36] R.Wei: Plasma enhanced magnetron sputtering deposition of superhard, nanocomposite coatings, Chapter 3 in *Plasma Surface Engineering Research and its Practical Applications*, R.Wei (Ed.), Kerala, Research Signpost Publisher, 2008, pp. 87-115.
[37] A.D.Pogrebjank, A.P.Shpak, N.A.Azarenkov and V.M.Beresnev: Structure and properties of hard and superhard nanocomposite coatings, Phys.Usp. 52 (2009), 29-54.
[38] A.Matthews and A.Leyland: Materials related aspects of nanostructured tribological coatings, SVC Bulletin, Spring 2009, pp. 40-44.
[39] A.D.Korotaev, B.D.Borisov, Yu.V.Moshkov, S.V.Ovchinnikov, Yu.P.Pinzhin, A.N.Tyumentsev: Elastic stress state in superhard multielement coatings, Physical Mesomechanics 12(5-6) (2009), 269-279 (in Russian).
[40] J.Musil: Recent progress in hard nanocomposite coatings, Part 1, Galvanotechnik 8 (2010), 1856-1867, Part 2, Galvanotechnik 9 (2010), 2116-2121.
[41] J.Musil: Hard nanocomposite coatings: Thermal stability, oxidation resistance and toughness, Surf.Coat.Technol. 207 (2012), 50-65.
[42] J.Musil, P.Zeman, P.Baroch: Hard Nanocomposite Coatings, in *Comprehensive Materials Processing, Volume 4, Coatings and Films, Chapter 4.13*, D.Cameron (Ed.), Elsevier, 2014, pp. 325-353.
[43] S.Veprek: Recent search for new superhard materials: Go nano!, J.Vac.Sci.Technol. A31 (5) (2013), 050822-1-33.
[44] J.Musil: Advanced hard nanocomposite coatings with enhanced toughness and resistance to cracking, Chapter 7 in *Thin Films and Coatings: Toughening and Toughening Characterization,* S.Zhang (Editor) CRC Press, USA, 2015, pp. 377-463.
[45] [37] J.Blažek, J.Musil, P.Stupka, R.Čerstvý and J.Houška: Properties of nanocrystalline Al-Cu-O films reactively sputtered by dc pulse dual magnetron, Applied Surface Science 258 (2011), 1762-1767.
[46] J.Musil, J.Sklenka, R.Cerstvy: Transparent Zr-Al-O nanocomposite coatings with enhanced resistance to cracking, Surf.Coat.Technol. 206 (2012), 2105-2109.

[47] J.Musil, M.Meissner, R.Jilek, T.Tolg, R.Cerstvy: Two-phase single layer Al-O-N nanocomposite films with enhanced resistance to cracking, Surf.Coat.Technol. 206 (2012), 4230-4234.
[48] J.Musil, J.Sklenka, R.Čerstvý, T.Suzuki, M.Takahashi, T.Mori: The effect of addition of Al in ZrO2 thin film on its resistance to cracking, Surf. Coat.Technol. 207 (2012), 355-360.
[49] J.Musil, J.Sklenka, J.Prochazka: Protective over-layer coating preventing cracking of thin films deposited on flexible substrates, Surf. Coat.Technol. 240 (2014), 275-280.
[50] J.Musil, R.Jílek, R.Čerstvý: Flexible Ti-Ni-N thin films prepared by magnetron sputtering, Journal of Materials Science and Engineering A 4(2) (2014), 27-33.
[51] J.Musil, J.Blazek, K.Fajfrlik, R.Cerstvy: Flexible antibacterial Al-Cu-N films, Surf.Coat.Technol. 264 (2015), 114-120.
[52] J.Prochazka, R.Cerstvy, J.Musil: Interrelationship between mechanical properties and resistance to cracking of magnetron sputtered (Ti,Al,V)N_x nitride films, Paper B5-1-4, 42nd international Conference on Metallurgical Coatings and Thin Films (ICMCTF 2015), April 20-24, 2015, San Diego, CA, USA, Book of Abstracts, p.80.
[53] *Thin Films Processes*, J.L.Vossen, W.Kern (Eds.), Academic Press, Inc., New York, 1978.
[54] B.Window, N.Savvides: Unbalanced magnetrons as sources of high ion fluxes, J.Vac.Sci.Technol. A4 (1986), 504.
[55] S.Kadlec, J.Musil, J.Vyskocil: Hysteresis effect in reactive sputtering: a problem of system stability, J.Phys.D: Appl.Phys. 19 (1986), L 187-L 190.
[56] S.Schiller, U.Heisig, Chr.Korndorfer, G.Beister, J.Reske, K.Steinfelder, J.Strumpfel: Reactive DC high-rate sputtering as production technology, Surf.Coat.Technol. 33 (1987), 405-423.
[57] J.Musil, S.Kadlec, J.Vyskocil, V.Valvoda: New results in dc reactive magnetron deposition of TiN_x films, Thin Solid Films 167 (1988), 107-119.
[58] *Handbook ofPlasma Processing Technology*, S.M.Rossnagel, J.J.Cuomo, W.D.Westwood (Eds.), Noyes Publications, Park Ridge, New Jersey, USA, 1990.
[59] B.Window, N.Savvides: Ion-assisting magnetron sources: Principles and uses, J.Vac.Sci.Technol. A8 (1990), 1277.
[60] J.Musil, S.Kadlec, V.Valvoda, R.Kuzel,Jr., R.Cerny: Ion-assisted sputtering of TiN films, Surf.Coat. Technol. 43/44 (1990), 259-269.
[61] J.Musil, S.Kadlec, W.-D.Munz: Unbalanced magnetrons and new sputtering systems with enhanced plasma ionization, J.Vac.Sci.Technol. A 9(3) (1991), 1171-1177.
[62] E.Kusano: An investigation of hysteresis effects as a function of pumping speed, sputtering current, and O_2/Ar ratio, in Ti-O_2 reactive sputtering processes, J.Appl.Phys. 70(11) (1991), 7089-1700.
[63] S.L.Rohde, L., Hultman, M.S.Wong, W.D.Sproul: Dual-unbalanced magnetron deposition of tiN films, Surf.Coat.Technol. 50 (1992), 255-262.
[64] J.Musil, S.Kadlec, J.Vyskocil: Hard coatings prepared by sputtering and arc evaporation in *Physics of Thin Films*, Mechanic and dielectric properties, Vol. 17, M.H.Fracombe, J.L.Vossen (Eds.), Academic Press, Inc. San Diego, CA, 1993, pp. 80-139.
[65] S. Schiller, K. Goedicke, J. Reschke, V. Kirchhoff, S. Schneider and F. Milde: Pulsed magnetron sputter technology, *Surf. Coat. Technol.*, 61 (1-3) (1993) 331-337.
[66] W.D.Sproul: Ion-assisted deposition in unbalanced-magnetron sputtering systems, Materials Science and Engineering A163 (1993), 187-192.
[67] S.M.Rossnagel: Directional and preferential sputtering-based physical vapour deposition, Thin Solid Films 263 (1995), 1-12.
[68] W.D.Sproul: Advances in reactive sputtering, 39th Annual Technical Conference Proceedings, Philadelphia,USA, 1996, pp. 3-6.
[69] W.D.Sproul: New routes in the preparation of mechanically hard films, Science 273 (1996), 889-892.
[70] B.Window: Issues in magnetron sputtering of hard coatings, Surf.Coat.Technol. 81 (1996), 92-98.
[71] S.Kadlec, J.Musil; Low pressure magnetron sputtering and selfsputtering discharges, Vacuum 47(3) (1996), 307-311.
[72] J.Musil: Basic properties of low-pressure plasma, in *Proceedings of the International School of Physics Enrico Fermi, Course CXXXV*, A.Paoleti and A.Tucciarone (Eds.), IOS Press, Amsterdam 1997, 145-177
[73] W.D.Sproul: High-rate reactive DC magnetron sputtering of oxide and nitride superlattice coatings, Vacuum 51(40 (1998), 641-649.
[74] J.Musil: Low-pressure magnetron sputtering, Vacuum 50 (3-4) (1998), 363-372
[75] R.D. Arnell, P.J.Kelly: Recent advances in magnetron sputtering, Surf.Coat.Technol. 112 (1999), 170-176.
[76] I.Safi: Recent aspects concerning DC reactive magnetron sputtering of thin films: a review, Surf.Coat. Technol. 127 (2000), 203-218.
[77] P.J.Kelly, R.D.Arnell: Magnetron sputtering: a review of recent developments and applications, Vacuum 56 (2000), 159-172.

[78] J.Musil: Hard nanocomposite films prepared by reactive magnetron sputtering, Chapter 5 in *Nanostructured Thin Films and Nanodispersion Strengthened Coatings*, A.A.Voevodin, D.V.Shtansky E.A.Levashov, J.J.Moore (Eds.) NATO Science Series, Vol.155, Kluwer Academic Publishers, Dordrecht, The Netherlands, 2003, pp.43-57.
[79] W.D.Sproul, D.J.Christie, D.C.Carter: Control of reactive sputtering processes: review, Thin Solid Films 491 2005), 1-17.
[80] J.Musil, J.Vlček, P.Baroch: Magnetron discharges for thin films plasma processing, Chapter 3 in „*Materials Surface Processing by Directed Energy Techniques*, Y.Pauleau (Ed.), 2006, Elsevier Science Publisher B.V., Oxford, UK, pp. 67-106.
[81] J.Musil, P.Baroch: High-rate pulse reactive magnetron sputtering of oxide nanocomposite coatings, Vacuum 87 (2013), 96-102.
[82] J.Musil, P.Baroch: Discharge in dual magnetron sputtering system, IEEE Trans on Plasma Science, 33(2) (2005), 338-339.
[83] H.Polakova, J.Musil, J.Vlcek, J.Alaart, C.Mitterer: structure-hardness relations in sputtered Ti-Al-V-n films, Thin Solid Films 444 (2003), 189-198.
[84] J.Musil: Sputtering systems with enhanced ionization for ion plating of hard wear resistant coatings, Proc. of the 1st Meeting on the Ion Engineering Society of Japan (IESJ-92), Tokyo, Japan, 1992, pp. 295-304.
[85] H.Poláková, J.Musil, J.Vlček, J.Alaart, C.Mitterer: Structure- hardness relations in sputtered Ti-Al-V-N films, Thin Solid Films 444 (2003), 189-198.
[86] J.Musil, H.Polaková, J.Šůna, and J.Vlček: Effect of ion bombardment on properties of hard reactively sputtered single-phase films, Surf.Coat.Technol. 177-178 (2004), 289-298.
[87] J.Musil, and J.Šůna: The role of energy in formation of sputtered nanocomposite films, Materials Science Forum 502 (2005), 291-296.
[88] J.Musil, J.Šícha, D.Heřman, R.Čerstvý: Role of energy in low-temperature high-rate formation of hydrophilic TiO_2 thin films using pulsed magnetron sputtering, J. Vac. Sci. Technol. A 25(4) (2007), 666-674.
[89] J. Musil, J.Lestina, J.Vlcek, T.Tolg: Pulsed dc magnetron discharge for high-rate sputtering of thin films, J.Vac. Sci.Technol., A19 (2001), 420-424.
[90] J. Vlcek, A.D. Pajdarova and J. Musil: Pulsed dc magnetron discharges and their utilization in plasma surface engineering, Cont. Plasma Phys., 44 (5–6) (2004) 426-436.
[91] R.D.Arnell, P.J.Kelly, J.W.Bradley: Recent developments in pulsed magnetron sputtering, Surf.Coat. Technol. 188-189 (2004), 158-163.
[92] A.P.Ehiasarian: Fundamentals and applications of HIPIMS, Chapter 2, in *Plasma Surface Engineering Research and its Practical Applications*, R.Wei (Ed.), Kerala, Research Signpost Publisher, 2008, pp. 35-86.
[93] A.Anders, J.Andersson, A.Ehiasarian: High power impulse magnetron sputtering: Current-voltage-time characteristics indicate the onset of self-sputtering, J.Appl.Phys. 102 (2007) 113303-p1 -p11.
[94] U.Helmersson, M.Lattemann, J.Bohlmark, A.P.Ehiasiaran: Ionized physical vapor deposition (IPVD): A review of technology and applications, Thin Solid Films 513 (1-2) (2006), 1-24.
[95] J.Vlcek, P.Kudlacek, K.Burcalova, J.Musil: High-power pulsed sputtering using a magnetron with enhanced plasma confinement, J.Vac.Sci.Technol. A25 (2007), 42-47.
[96] J.Vlcek, P.Kudlacek, K.Burcalova, J.Musil: Ion flux characteristics in high-power pulsed magnetron sputtering discharges, EPL 77 (2007), 45002- p1-p5.
[97] D.Horwat, A.Anders: Spatial distribution of average charge state and deposition rate in high power impulse magnetron sputtering of copper, J.Phys.D: Appl.Phys. 41 (2008), 135210 (6 pp).
[98] J.W.Bradley, T.Welzel: Physics and phenomena in pulsed magnetrons: an overview, J.Phys.D: Appl.Phys. 42 (2009), 093001 (23 pp).
[99] A.Anders: Deposition rates of high power impulse magnetron sputtering: Physics and economics, J.Vac.Sci.Technol. A28(4) (2010), 783-790.
[100] P.Poolcharuansin, J.Bradley: Shot- and long-term plasma phenomena in a HIPIMS discharge, Plasma Sources Sci.Technol. 19 (2010), 025010 (13 pp).
[101] A.Anders, M.Panjan, R.Franz, J.Andersson, P.Ni: Drifting potential humps in ionization zones: The "propeller blades" of high power impulse magnetron sputtering, Appl.Phys.Lett. 103 (2013), 144103 (4 pp).
[102] P.M.Barker, E.Lewin, J.Patscheider: Modified high power impulse magnetron sputtering process for increased deposition rate of titanium, J.Vac.Sci.Technol. A 31(6) (2013), 060604 (4 pp).
[103] J.Musil, J.Blažek, K.Fajfrlík, R.Čerstvý, Š.Prokšová: Antibacterial Cr-Cu-O films prepared by reactive magnetron sputtering, Applied Surface Science 276 (2013), 660-666.
[104] J.A.Thornton: (i) Recent developments in sputtering – Magnetron sputtering, Metal Finishing 77(5) (1979), 83-87 and (ii) High rate thick films growth, Ann. Rev. Mater. Sci. 7 (1977), 239-260.

[105] B.A.Movchan, A.V.Demchishin: Study of the structure and properties of thick vacuum condensates of nickel, titanium, tungsten, aluminum oxide and zirconium oxide, Phys. Met. Metallogr. 28 (1969), 83-90.
[106] J.Musil, V.Poulek, V.Valvoda, R.Kužel Jr., H.A.Jehn, M.E.Baumgartner: Relation of deposition conditions of Ti-N films prepared by dc magnetron sputtering to their microstructure and macrostress, Surf.Coat.Technol. 60 (1993), 484-488.
[107] P.Pokorny, J.Musil, P.Fitl, M.Novotny, J.Lancok, J.Bulir: Contamination of magnetron sputtered metallic films by oxygen from residual atmosphere in deposition chamber, Plasma Processes and Polymers (2015); online 28 Dec 2014/doi: 10.1002/ppap.201400172, in press.
[108] R.Messier, A.P.Giri, R.A.Roy: Revised structure zone model for thin film physical structure, J.Vac.Sci.Technol. A2(2) (1984), 500-503.
[109] A.Anders: A structure zone diagram including plasma-based deposition and ion etching, Thin Solid Films 518 (2009), 4087-4090.